


 Cite this: *RSC Adv.*, 2025, **15**, 6742

Trinuclear cylinder-like potential anticancer and antibacterial Cu(i), Ag(i) and Au(i) nano-sized cationic complexes with tris-NHC ligands: cationic M₃ metal cluster displaying positive or negative cooperativity in triad [L₂(R)₆→M₃]³⁺ complexes?†

 Khadijeh Naeimi,^a Mehdi Bayat^{id *b} and Ehsan Alavi Pour^a

N-Heterocyclic carbenes (NHCs) are a class of organic molecules containing a divalent carbon atom, known as a carbene, within a heterocyclic (ring) structure where nitrogen atoms (N) form part of the ring. These molecules have garnered significant attention in coordination chemistry due to their unique bonding properties, particularly as strong σ -donor ligands that facilitate the formation of stable complexes. A theoretical study was conducted to investigate the structural and bonding characteristics of M←C bonds in trinuclear, nano-sized Cu(i), Ag(i), and Au(i) cations with two tris-NHC ligands, which exhibit promising anti-cancer and antibacterial potential. The study employed natural bond orbital (NBO) techniques, energy decomposition analysis (EDA), and extended transition-state natural orbital for chemical valence (ETS-NOCV) methods to analyze the bonding interactions. The cooperativity values between bonds were also examined, revealing positive values indicative of anti-cooperativity within the complexes. The results further demonstrated that the M←C interactions are predominantly electrostatic in nature. These findings highlight the unique structural and electronic properties of the complexes, suggesting their potential as candidates for anti-cancer and antibacterial applications.

 Received 3rd December 2024
 Accepted 24th February 2025

 DOI: 10.1039/d4ra08514k
rsc.li/rsc-advances

Introduction

N-Heterocyclic carbenes (NHCs) have emerged as versatile ligands in both organometallic and inorganic chemistry. Owing to their strong σ -donating properties, NHCs form more stable bonds with metals than phosphines,¹ with the lone pair of electrons on the carbene carbon stabilized by adjacent nitrogen atoms through an inductive effect.² Additionally, metal–NHC complexes have attracted significant attention due to their wide range of catalytic^{3,4} and pharmacological^{5–7} properties. They are extensively used as ligands in inorganic and organometallic chemistry for two primary reasons: first, their strong metal coordination, and second, their resistance to moisture and air.^{2,8} As a result, NHCs are preferred as substitutes for phosphine ligands. Modifications at the (N₁) position of the NHC ligand significantly impact its reactivity and binding affinity. Transition metal–NHC complexes have been employed in medicinal chemistry due to their remarkable biological

properties.⁹ N-heterocyclic carbene–metal complexes have gained significance in fields like organometallic chemistry, catalysis and bioorganic/bioinorganic chemistry. Among these, coinage metal–NHCs are particularly noteworthy due to their varied biological properties and applications.^{10,11} The NHC copper complexes have the potential to generate reactive oxygen species (ROS), which can cause DNA strand breaks and contribute to the observed cytotoxicity.¹² Metallic silver was recognized by the Chaldeans as early as 4000 B.C.E., making it the third metal used by ancient civilizations, following gold and copper.¹³ Although most organometallic pharmaceutical research has focused on platinum and gold, the medicinal applications of silver are well-documented.¹⁴ Multinuclear silver N-heterocyclic carbene (Ag–NHC) complexes have garnered interest in medicinal chemistry due to their unique properties and potential applications. These complexes represent a promising area in medicinal chemistry, with potential applications in antimicrobial and anticancer therapies.^{15–19} Gold has long been essential in human history. Likely the first metal to be discovered, it has been utilized in medicinal treatments since ancient times.²⁰ Multinuclear gold–N-heterocyclic carbene (Au–NHC) complexes are an evolving area of research in medicinal chemistry, showing promise for various therapeutic applications. These complexes are emerging as a promising class of compounds in medicinal chemistry. They hold potential for

^aDepartment of Inorganic Chemistry, Faculty of Chemistry and Petroleum Sciences, Bu-Ali Sina University, Hamedan, Iran

^bSchool of Chemistry, College of Science, University of Tehran, Tehran, Iran. E-mail: bayatm@ut.ac.ir; mehdi806@gmail.com

† Electronic supplementary information (ESI) available. See DOI: <https://doi.org/10.1039/d4ra08514k>



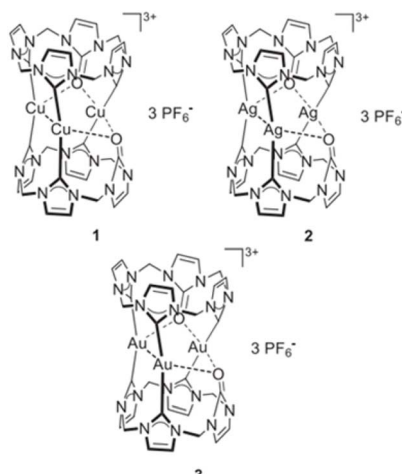


Fig. 1 The structure of the pharmaceutical complexes studied by Jacob.

applications in both cancer therapy and antimicrobial treatments.^{21–26} In 2021, Jacob reported the synthesis and identification of the first large cyclic trinuclear, tri-carbene complexes Cu(i), Ag(i), and Au(i). The ability of these complexes to inhibit the growth of bacteria (*S. aureus*, *E. coli*) and cancer cells (HeLa, MCF7) was investigated. The copper and silver complexes demonstrated antiproliferative activity in both cell lines, ranging from 3.03 μM to 25.01 μM (ref. 27) (see Fig. 1).²⁷ Compared to mononuclear complexes, multinuclear complexes have more active sites that can coordinate with substituents possessing biological properties, and as a result, they may exhibit stronger biological activities.²⁸

Recent studies have investigated the structure and nature of metal–NHC bonds in some pharmaceutical coinage metal ion complexes.^{29–33} Cooperativity in bonds refers to the phenomenon where the formation, breaking, or alteration of one bond influences the behavior of nearby bonds. This interaction can enhance or inhibit subsequent bonding events, depending on the system. Cooperativity is widely observed in physical, chemical, and biological systems, and it is particularly important in stabilizing molecular structures and driving complex reactions. Herein, a comparative theoretical investigation into the nature of the metal–NHC bonds of some cylindrical trinuclear clusters of group 11 in coordination with two symmetrical tri-N-heterocyclic carbene (NHC) ligand was reported. The effect of substituents, C_2H_5 , CH_3 , H, F, Cl, Br, Ph, and SiH_3 on six NHC rings of cationic three-metal clusters of copper (1), silver (1) and gold (1) are also investigated. It is worth noting that the X-ray crystal structures of three metal clusters, copper, silver and gold, substituted with C_2H_5 were synthesized by Rit in 2010 (ref. 34) and 2011.³⁵ Our research group has used the crystal structure of these clusters as input files for the calculations in this study Fig. 2.

Computational details

The $[\text{L}_2(\text{C}_2\text{H}_5)_6 \rightarrow \text{Au}_3]^{3+}$ complex is analysed using eight density functional methods: Cam-B3LYP, M05-2X, M06-2X, B3LYP,

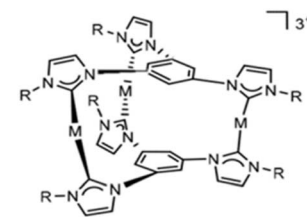


Fig. 2 Schematic representation of the $[\text{L}_2(\text{R})_6 \rightarrow \text{M}_3]^{3+}$ nano-sized cationic complexes.

Table 1 RMS calculation of $[\text{L}_2(\text{C}_2\text{H}_5)_6 \rightarrow \text{Au}_3]^{3+}$ complex

Method	Au–C (Å)	Au–C (Å)	Au–C (Å)	RMS
B3LYP-D3	2.06	2.06	2.06	0.09
BLYP-D3	2.06	2.06	2.06	0.09
BP86-D3	2.04	2.04	2.04	0.06
CAM-B3LYP-D3	2.05	2.05	2.05	0.08
M05-2X-D3	2.05	2.05	2.05	0.08
M06-D3	2.06	2.06	2.06	0.09
M06-2X-D3	2.05	2.05	2.05	0.08
PBE-D3	2.04	2.04	2.04	0.06
Exp	2.00	2.01	2.00	—

PBE,³⁵ BLYP, BP86 and M06, in conjunction with D3 dispersion corrections. Additionally, the structural results obtained were compared with the corresponding experimental values derived from X-ray crystallography.^{34,35} The results obtained from the RMS methodological findings indicate that PBE-D3,³⁶ the most relevant functional among the methods mentioned, shows the strongest correlation between quantitative and experimental structural data in Table 1.

In this article, the cationic parts of the complexes with the general formula $[\text{L}_2(\text{R})_6 \rightarrow \text{M}_3]^{3+}$ (where $\text{M} = \text{Cu(i)}, \text{Ag(i)}, \text{Au(i)}$; $\text{R} = \text{C}_2\text{H}_5, \text{CH}_3, \text{H}, \text{F}, \text{Cl}, \text{Br}, \text{Ph}$, and SiH_3) were investigated. All calculations (optimized structures and single points) were performed at the PBE-D3/def2-TZVP^{37,38} level of theory using Gaussian 09 software.³⁹ All structures were optimized and their energies were obtained in gas phase using PBE-D3/def2-TZVP level of theory. The vibrational frequency analysis indicates that the optimized structures at stationary points, obtained at the same theoretical level, correspond to local minima, as evidenced by the absence of imaginary frequencies. NBO analysis calculations were performed to investigate the nature of the

$\text{C}_{(\text{tris-NHC})} \rightarrow \text{M}_3$ bonds using the Gaussian 09 at the BP86/def2-TZVP theoretical level.^{40,41} Energy decomposition analysis (EDA) was conducted to assess the nature of the $\text{C}_{(\text{tris-NHC})} \rightarrow \text{M}_3$ bonds at the BP86-D3/TZ2P level of theory, utilizing the ADF 2013.01 software package.

Result and discussion

Structural studies

The mentioned complexes optimized on PBE-D3/def2TZVP level of theory in the gas phase. The optimized structures and length of the corresponding of $[\text{L}_2(\text{R})_6 \rightarrow \text{M}_3]^{3+}$ complexes; $\text{M} = \text{Cu(i)}$,



Ag(i), Au(i); R = C₂H₅ and CH₃ are shown in Fig. 3. The optimized structure of the other related complexes has been reported in the Tables S3 and S4.†

To measure the length of complexes, [L₂(R)₆→M₃]³⁺; M = Cu(i), Ag(i), Au(i); R = H, F, Cl, Br, CH₃ and SiH₃, the distance between two atoms H, F, Cl, Br, C, and Si located on reciprocal R's was calculated. Similarly, for complexes [L₂(R)₆→M₃]³⁺; M = Cu(i), Ag(i), Au(i); R = C₂H₅ and Ph, the distance between two distant carbon atoms located on R was measured.

Structural data confirmed that this series of complexes has a nanostructure sized (see Fig. 3–5). All coordination details of the Au(i); R = C₂H₅, CH₃, H, F, Cl, Br, Ph, and SiH₃, were 1.90 Å for information. Optimized complexes mentioned are provided in the supporting copper complexes and 2.08 Å for silver complexes. Also, C_(tris-NHC)→M₃ bond lengths for the gold complexes are approximately 2.03 Å. According to the results, a reverse V-shaped trend is observed. With the change in substituents, no significant changes are observed. Due to the symmetrical nature of the studied complexes, the bond length of each of the six C_(tris-NHC)→M₃ bonds in each complex

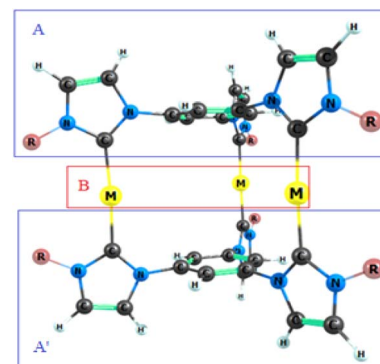


Fig. 4 Fragments analysis of [L₂(R)₆→M₃]³⁺ complexes investigated here.

remains the same. Therefore, only one bond length for the C_(tris-NHC)→M₃ bond is reported. The bond lengths of the C_(tris-NHC)→M₃ bonds in the mentioned complexes are listed in the ESI, Table S1.†

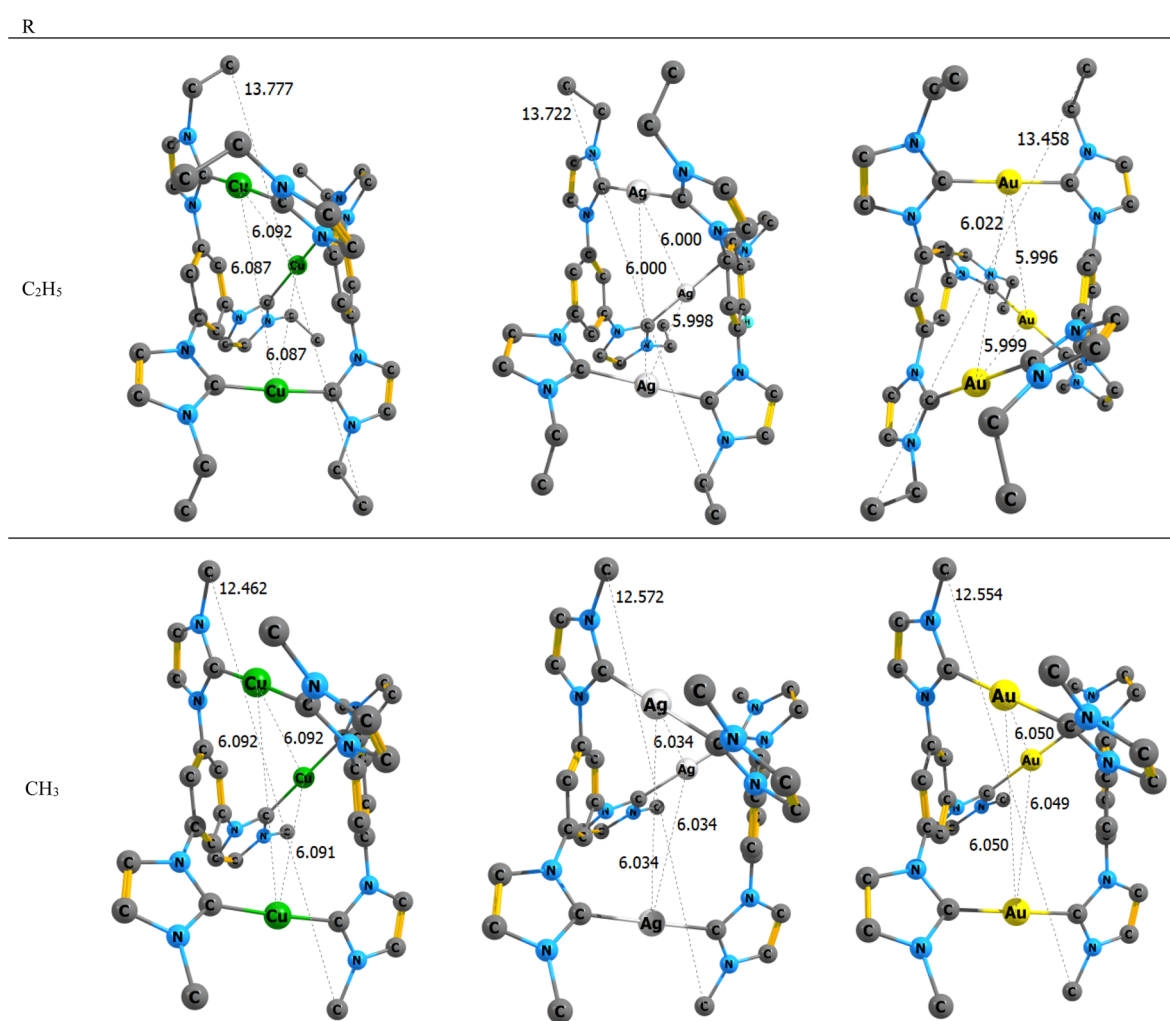
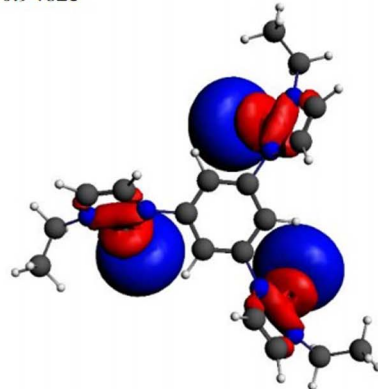


Fig. 3 The optimized structures and length of [L₂(R)₆→M₃]³ complexes; M = Cu(i), Ag(i), Au(i); R = C₂H₅ and CH₃. All hydrogen atoms were removed to enhance clarity.

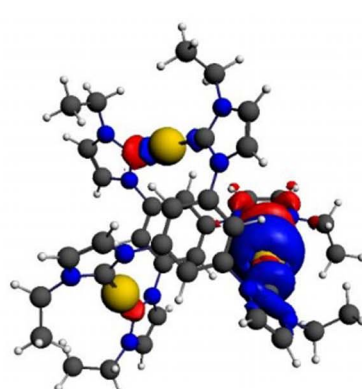


Component A-B of $[L_2(Ph)_6 \rightarrow Ag_3]^{3+}$

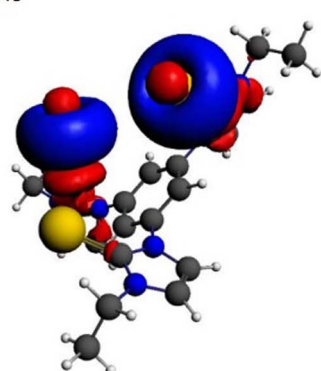
$\Delta\rho_1$ $\Delta E = -67.24$ kcal/mol
v: 0.94825

Component A-BA' of $[L_2(Ph)_6 \rightarrow Ag_3]^{3+}$

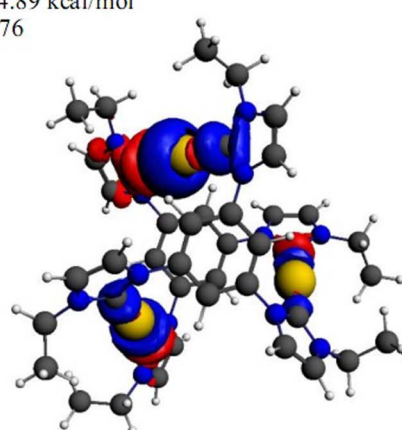
$\Delta E = -44.99$ kcal/mol
v: 0.56493



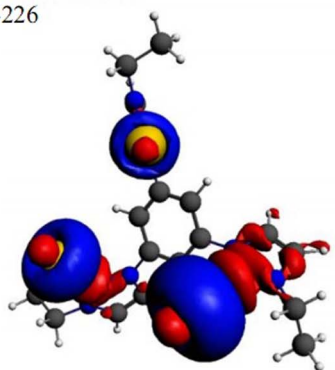
$\Delta\rho_2$ $\Delta E = -66.91$ kcal/mol
v: 0.94245



$\Delta E = -44.89$ kcal/mol
v: 0.56476



$\Delta\rho_3$ $\Delta E = -66.86$ kcal/mol
v: 0.94226



$\Delta E = -44.89$ kcal/mol
v: 0.56473

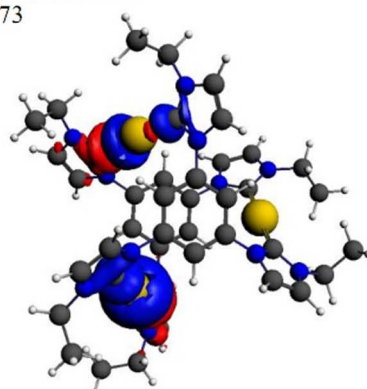


Fig. 5 Contour plots of NOCV deformation densities $\Delta\rho$ and associated energies $\Delta E(\rho)$, computed at the BP86-D3/TZ2P level of theory. The corresponding deformation electron densities were depicted by the direction of charge transitioning from red to blue. The eigenvalues (v) give the size of the charge migration.

Interaction energy

The interaction energies between the examined M_3^{3+} ions and the ligand fragments in the optimized structures of the nano-sized complexes were calculated using the PBE/def2-TZVP

level of theory. The results are shown in Table 2. To calculate the interaction energy in the complexes $[L_2(R)_6 \rightarrow M_3]^{3+}$, three fragments A, A', and B were defined as follows Fig. 4. In this study, the interaction energy between fragments A and B, as well



Table 2 Interaction energy (IE) (kcal mol⁻¹) of $[L_2(R)_6 \rightarrow M_3]^{3+}$ complexes

M	R	IE _{A-B} ^{ABA'}	IE _{B-A} ^{ABA'}	IE _{A-B-A'} ^{ABA'}	IE _{AB-A'} ^{ABA'}	IE _{total(eqn (1))}	IE _{total(eqn (2))}
Cu	C ₂ H ₅	-360.60	-360.60	-272.42	-272.42	-633.02	-633.02
	CH ₃	-353.73	-353.73	-270.31	-270.31	-624.04	-624.04
	H	-341.57	-341.56	-267.69	-267.68	-609.25	-609.25
	F	-311.61	-311.62	-251.54	-251.55	-563.16	-563.16
	Cl	-330.02	-330.02	-259.21	-259.21	-589.23	-589.23
	Br	-336.10	-336.10	-261.11	-261.11	-598.11	-598.11
	SiH ₃	-358.89	-358.89	-271.66	-271.66	-630.55	-630.55
	Ph	-373.52	-373.09	-277.89	-277.46	-650.98	-650.98
Ag	C ₂ H ₅	-318.43	-318.43	-244.87	-244.87	-563.30	-563.30
	CH ₃	-308.74	-308.74	-240.28	-240.27	-549.01	-549.01
	H	-305.49	-305.49	-247.25	-247.25	-552.74	-552.74
	F	-268.23	-268.23	-222.27	-222.27	-490.50	-490.50
	Cl	-289.92	-289.93	-232.30	-232.32	-522.24	-522.24
	Br	-293.81	-293.80	-232.19	-232.18	-525.99	-525.99
	SiH ₃	-312.10	-312.10	-242.03	-242.02	-554.12	-554.12
	Ph	-328.82	-328.82	-246.73	-246.73	-575.55	-575.55
Au	C ₂ H ₅	-439.04	-438.66	-304.27	-303.89	-742.93	-742.93
	CH ₃	-429.20	-429.21	-301.16	-301.17	-730.37	-730.37
	H	-415.94	-415.95	-300.52	-300.53	-716.48	-716.48
	F	-380.23	-380.23	-284.79	-284.79	-665.02	-665.02
	Cl	-402.31	-402.32	-291.90	-291.90	-694.21	-694.21
	Br	-411.16	-411.16	-293.81	-293.81	-704.97	-704.97
	SiH ₃	-434.76	-434.79	-303.19	-303.22	-737.98	-737.98
	Ph	-449.84	-449.30	-307.12	-306.57	-756.41	-756.41

as A and A'B, was investigated. Single point (SP) energy of all fragments, (A, B, A', AB and A'B) were calculated using the PBE/def2-TZVP level of theory. Due to the symmetry of the complex, the interaction energy was analysed for only one side of the complex. The interaction energy was measured according to the following equations.⁴² The total interaction energy was calculated using two formulas, eqn (1) and eqn (2). The total interaction energies obtained from both formulas are same.

$$IE_{\text{Total}}^A = \frac{1}{2}(IE_{A-B} + IE_{B-C} + IE_{A-BC} + IE_{AB-C}) \quad (1)$$

$$IE_{\text{Total}}^B = E_{ABC} - (E_A^{ABC} + E_B^{ABC} + E_C^{ABC}) \quad (2)$$

Results indicated that the interaction energy values for Cu(i), Ag(i) Au(i); in $[L_2(R)_6 \rightarrow M_3]^{3+}$ complexes were in the ranges of (-563.16 to -650.98) kcal mol⁻¹, (-490.50 to -575.55) kcal mol⁻¹ and (-665.02 to -756.41) kcal mol⁻¹ respectively. Assuming R is constant, the trend of total interaction energy for group 11 metals is V-shaped, IE Au(1) > IE Cu(1) > IE Ag(1). For example, the total interaction energy for the complexes $[L_2(C_2H_5)_6 \rightarrow Au_3]^{3+}$, $[L_2(RC_2H_5)_6 \rightarrow Ag_3]^{3+}$ and $[L_2(C_2H_5)_6 \rightarrow Cu_3]^{3+}$ were -742.93 kcal mol⁻¹, -563.30 kcal mol⁻¹ and -633.02 kcal mol⁻¹, respectively. Changing the substituent on the NHC rings alters the interaction energy. The total interaction energies for electron-donating substituents, such as Ph, C₂H₅, and CH₃, are higher than those for electron-withdrawing substituents such as F, Cl, and Br. This trend was observed across all three metal clusters investigated. Additionally, the highest and lowest total interaction energies were associated with the complexes $[L_2(Ph)_6 \rightarrow Au_3]^{3+}$,

which has an interaction energy of -756.41 kcal mol⁻¹, and $[L_2(F)_6 \rightarrow Ag_3]^{3+}$, which has an interaction energy of -490.50 kcal mol⁻¹.

Cooperativity

In 1957 Frank and Wen⁴³ qualitatively described the presence of cooperative effects among hydrogen bonds as a nonadditive enhancement of interactions through the formation of additional bonds. Significant attention has been focused on cooperativity within a triad formed by noncovalent interactions among three connected monomers⁴⁴ Hanks⁴⁵ and colleagues proposed a characteristic feature of the cooperative effect in a triadic configuration of H₂O molecules, treating it as a noncyclic A-B-C system based on the concept of "pairwise nonadditivity" represented by the following equation: eqn (3)

$$E_{\text{coop}} = SE_{ABC} - SE_{AB} - SE_{BC} - SE_{(AC, T)} \quad (3)$$

SE_{ABC} denotes the stabilization energy of the triad, while SE_{AB} and SE_{BC} represent the stabilization energies of the isolated dyads within their respective minima configurations. The term SE_(AC, T) also signifies the stabilization energy of molecules A and C in the triad configuration. However, while several theoretical studies⁴⁶⁻⁵¹ have calculated the cooperative energy using eqn (3) and other studies have employed eqn (4), which does not take SE_(AC, T) into account.⁵²⁻⁵⁶

$$E_{\text{coop}} = SE_{ABC} - SE_{AB} - SE_{BC} \quad (4)$$

Cooperativity refers to the phenomenon where multiple interactions within a system influence each other, causing the



system to behave differently than would be expected from the individual interactions acting alone. This coupling can result in either positive cooperativity (where one interaction enhances another) or negative cooperativity (where one interaction reduces another). It is a fundamental aspect of systems chemistry that produces collective properties not found in the individual components.⁵⁷ One example of cooperativity is hemoglobin, where the binding of oxygen to one site increases the affinity of the other sites for oxygen.⁵⁸ In 2024, Sanei Movafagh and co-workers introduced a new equation eqn (5) for calculating cooperativity based on bond interaction energy in three-component systems.⁵⁵

$$\begin{aligned}\Delta E_{\text{coop}} &= \Delta E_{\text{A-B}} = \Delta E_{\text{B-C}} \\ \Delta E_{\text{A-B}} &= IE_{\text{A-BC}}^{\text{ABC}} - IE_{\text{A-B}}^{\text{ABC}} \\ \Delta E_{\text{B-C}} &= IE_{\text{AB-C}}^{\text{ABC}} - IE_{\text{B-C}}^{\text{ABC}}\end{aligned}\quad (5)$$

The calculated values of the cooperativity energy based on eqn (5) for the nano-sized complexes $[\text{L}_2(\text{R})_6 \rightarrow \text{M}_3]^{3+}$; $\text{M} = \text{Cu(i)}, \text{Ag(i)}, \text{Au(i)}$ and $\text{R} = \text{C}_2\text{H}_5, \text{CH}_3, \text{H}, \text{F}, \text{Cl}, \text{Br}, \text{Ph}$, and SiH_3 are summarized in Table 3. Based on the results, the cooperativity values for all complexes are positive, indicating the presence of anti-cooperativity. The trend of cooperativity for group 11 metals, similar to the interaction energy, exhibits a V-shaped pattern and follows the order, $\text{Ag(i)} < \text{Cu(i)} < \text{Au(i)}$. For example, cooperativity energy for the complexes $[\text{L}_2(\text{F})_6 \rightarrow \text{Cu}_3]^{3+}$, $[\text{L}_2(\text{F})_6 \rightarrow \text{Ag}_3]^{3+}$ and $[\text{L}_2(\text{F})_6 \rightarrow \text{Au}_3]^{3+}$ were 73.88 kcal mol⁻¹, 58.24 kcal mol⁻¹ and 115.42 kcal mol⁻¹, respectively.

Table 3 Cooperativity energy (kcal mol⁻¹) of $[\text{L}_2(\text{R})_6 \rightarrow \text{M}_3]^{3+}$ complexes

M	R	$IE_{\text{A-B}}^{\text{ABA'}}$	$IE_{\text{A-BA'}}^{\text{ABA'}}$	E_{coop}
Cu	C_2H_5	-360.60	-272.42	88.18
	CH_3	-353.73	-270.31	83.42
	H	-341.57	-267.69	73.88
	F	-311.61	-251.54	60.07
	Cl	-330.02	-259.21	70.81
	Br	-336.1	-261.11	74.99
	SiH_3	-358.89	-271.66	87.23
Ag	Ph	-373.52	-277.89	95.63
	C_2H_5	-318.43	-244.87	73.56
	CH_3	-308.74	-240.28	68.46
	H	-305.49	-247.25	58.24
	F	-268.23	-222.27	45.96
	Cl	-289.92	-232.30	57.62
	Br	-293.81	-232.19	61.62
Au	SiH_3	-312.1	-242.03	70.07
	Ph	-328.82	-246.73	82.09
	C_2H_5	-439.04	-304.27	134.77
	CH_3	-429.2	-301.16	128.04
	H	-415.94	-300.52	115.42
	F	-380.23	-284.79	95.44
	Cl	-402.31	-291.9	110.41
Au	Br	-411.16	-293.81	117.35
	SiH_3	-434.76	-303.19	131.57
	Ph	-449.84	-307.12	142.72

NBO analysis

In this study, we used Gaussian 09 software for NBO analysis. NBO analysis was utilized to quantify various bond parameters and to characterize the metal–ligand interactions. Based on NBO calculation at the PBE-D3/def2-TZVP level of theory, the nature of the $\text{C}_{(\text{tris-NHC})} \rightarrow \text{M}_3$ bonds in the mentioned nano-sized complexes were analysed.

Natural charge and charge transfer

The natural charge on M_3 atoms of the complexes $[\text{L}_2(\text{R})_6 \rightarrow \text{M}_3]^{3+}$; $\text{M} = \text{Cu(i)}, \text{Ag(i)}, \text{Au(i)}$; $\text{R} = \text{C}_2\text{H}_5, \text{CH}_3, \text{H}, \text{F}, \text{Cl}, \text{Br}, \text{Ph}$, and SiH_3 at the PBE-D3/def2-TZVP level of theory were collected. The results were shown in Table 4. In the complexes $[\text{L}_2(\text{R})_6 \rightarrow \text{M}_3]^{3+}$, the formal charges of the M_3 and $\text{L}_2(\text{R})_6$ fragments are +3 and 0, respectively. The results indicate that charge transfer occurs from the $\text{L}_2(\text{R})_6$ fragment to the M_3 . While the R substituent is constant, a decreasing trend in the natural charge was observed by changing the M from Cu(i) to Au(i). For example, the natural charges of the M_3 metal cluster in the complexes $[\text{L}_2(\text{Br})_6 \rightarrow \text{Cu}_3]^{3+}$, $[\text{L}_2(\text{Br})_6 \rightarrow \text{Ag}_3]^{3+}$ and $[\text{L}_2(\text{Br})_6 \rightarrow \text{Au}_3]^{3+}$ were found to be $1.17e$, $1.04e$, and $0.65e$, respectively. Additionally, the natural charge of the M_3 metal cluster is generally higher in the presence of electron-withdrawing substituents compared to electron-donating substituents. For example, the natural charges of complexes $[\text{L}_2(\text{F})_6 \rightarrow \text{Ag}_3]^{3+}$ and $[\text{L}_2(\text{C}_2\text{H}_5)_6 \rightarrow \text{Ag}_3]^{3+}$ were $1.21e$ and $1.04e$ respectively. The highest and lowest natural charges of the mentioned complexes correspond to the $[\text{L}_2(\text{F})_6 \rightarrow \text{Cu}_3]^{3+}$ and

Table 4 Natural charge and the amount of charge transfer $\text{L}_2(\text{R})_6 \rightarrow \text{M}_3$ for $[\text{L}_2(\text{R})_6 \rightarrow \text{M}_3]^{3+}$ complexes

M	R	Natural charge		Charge transfer
		M_3	$\text{L}_2(\text{R})_6$	$\text{L}_2(\text{R})_6 \rightarrow \text{Cu}_3$
Cu	C_2H_5	1.09	1.91	-1.91
	CH_3	1.09	1.91	-1.91
	H	1.14	1.86	-1.86
	F	1.25	1.75	-1.75
	Cl	1.20	1.80	-1.80
	Br	1.17	1.83	-1.83
	SiH_3	1.15	1.85	-1.85
Ag	Ph	1.16	1.84	-1.84
	C_2H_5	1.05	1.95	-1.95
	CH_3	1.05	1.95	-1.95
	H	1.11	1.89	-1.89
	F	1.21	1.79	-1.79
	Cl	1.10	1.90	-1.90
	Br	1.04	1.96	-1.96
Au	SiH_3	1.09	1.91	-1.91
	Ph	1.09	1.91	-1.91
	C_2H_5	0.61	2.39	-2.39
	CH_3	0.66	2.34	-2.34
	H	0.75	2.25	-2.25
	F	0.82	2.18	-2.18
	Cl	0.71	2.29	-2.29
Au	Br	0.65	2.35	-2.35
	SiH_3	0.68	2.32	-2.32
	Ph	0.67	2.33	-2.33



$[L_2(C_2H_5)_6 \rightarrow Au_3]^{3+}$, with values of 1.25 e and 0.61 e, respectively. The amount of charge transfer from $L_2(R_6)$ fragment to M_3 was also calculated. The results indicate an increasing trend in charge transfer when changing the M_3 from Cu(i) to Au(i) while keeping the same R substituent. For instance, the charge transfer amounts of $[L_2(Br)_6 \rightarrow Cu_3]^{3+}$, $[L_2(Br)_6 \rightarrow Ag_3]^{3+}$, and $[L_2(Br)_6 \rightarrow Au_3]^{3+}$ complexes are $-1.83e$, $-1.96e$ and $-2.35e$, respectively.

The results confirm that changing the metal from Cu(i) to Au(i) leads to a reduction in the natural charge on the M_3 . Also the complexes with electron-donating substituents exhibit greater amounts of charge transfer compared to those with electron-withdrawing substituents. Specifically, the highest and lowest charge transfer values correspond to $[L_2(C_2H_5)_6 \rightarrow Au_3]^{3+}$ and $[L_2(F)_6 \rightarrow Cu_3]^{3+}$ complexes which have charge transfers about $-2.39e$ and $-1.75e$, respectively.

Wiberg index

Using the Wiberg bond index (WBI) method, the chemical bond orders of $C_{(tris-NHC)} \rightarrow M_3$ in $[L_2(R)_6 \rightarrow M_3]^{3+}$ complexes; $M = Cu(i), Ag(i), Au(i)$ and $R = C_2H_5, CH_3, H, F, Cl, Br, Ph$ and SiH_3 are investigated. The results are summarized in Table S2 in the ESI.† Due to the symmetrical nature of the studied complexes, the bond order for each of the six $C_{(tris-NHC)} \rightarrow M_3$ bonds are same. Therefore, only one bond order for the $C_{(tris-NHC)} \rightarrow M_3$ bond is reported. By changing the M_3 from Cu(i) to Au(i) while keeping the same R substituents, a well-known V-shaped trend emerges for the Wiberg Bond Index (WBI) values of the $C_{(tris-NHC)} \rightarrow M_3$ bonds. This trend follows the order: $Ag(i) < Cu(i) < Au(i)$, which correlates well with the interaction energies. The results indicate that varying the substituents (R) does not affect the Wiberg index for the corresponding complexes.

Donor-acceptor and natural hybrid orbital (NHO) analysis

The results of the natural hybrid orbital (NHO) analysis for the M and C atoms in the $C_{(tris-NHC)} \rightarrow M_3$ bond within the $[L_2(R)_6 \rightarrow M_3]^{3+}$ complexes; $M = Cu(i), Ag(i), Au(i)$; $R = C_2H_5, CH_3, H, F, Cl, Br, Ph$ and SiH_3 are reported in Table 5. Apart from that, the occupancy of C atom in the latter bonds was $\approx 73\%$ in the presence of Au(i). For silver and copper, no occupancy of the C atoms in the latter bonds was observed. The modification of the R substituent does not significantly affect the occupancy values of carbon atoms in the $C_{(tris-NHC)} \rightarrow M_3$ bond. The calculated donor-acceptor interactions for the

investigated complexes are given in Table S3.† The results of indicate that the σ^* and Lp^* orbitals of M metal ion in the $C_{(tris-NHC)} \rightarrow M_3$ bonds are filled with the lone-pair electrons from the carbon atoms. The most significant and strong donor-acceptor interactions for Cu(i) and Ag(i) are observed as $C_{NHC} \rightarrow Cu(i)$ and $C_{NHC} \rightarrow Ag(i)$ transitions, which occur from the lone pair (LP) to the lone pair antibonding orbital (LP*). In the case of Au(i), the strongest interaction is from $C_{NHC} \rightarrow Au(i) - C_{NHC}$, transitioning from the lone pair (LP) to the sigma antibonding orbital (σ^*). These interactions highlight the varying nature of bonding in the metal complexes depending on the metal involved.

Energy decomposition analysis (EDA)

Energy decomposition analysis (EDA) is considered fundamental tool for obtaining information about the driving forces in molecular structure and for quantitatively interpreting chemical bonds. EDA calculations were performed based on the DFT method using the BP86-D3 functional and the TZ2P basis set on the relevant nano-sized complexes, utilizing ADF 2013 software. Four parameters are examined in the EDA calculations. The first parameter, ΔE_{pauli} , corresponds to the repulsive interactions between fragments, based on the fact that two electrons with similar spins cannot occupy the same region in space, which typically results in positive values. The second parameter, ΔE_{elstat} , determines the electrostatic interaction energy between the fragments, calculated using the frozen electron density distribution of the fragments in the molecular structure. The third parameter, ΔE_{orb} , includes covalent attraction in the M-L bonds. The fourth parameter, ΔE_{dis} , represents the change in energy due to dispersion interactions in a molecular system, arising from the attractive forces between temporary dipoles that form in molecules. These calculations were conducted to analyze the nature of the $C_{(tris-NHC)} \rightarrow M_3$ bond in the complexes $[L_2(R)_6 \rightarrow M_3]^{3+}$; ($M = Cu(i), Ag(i), Au(i)$ and $R = C_2H_5, CH_3, H, F, Cl, Br, Ph$ and SiH_3). The total interaction energy was calculated using the following equation eqn (6)

$$\Delta E_{int} = \Delta E_{elstat} + \Delta E_{orb} + \Delta E_{pauli} + \Delta E_{disp} \quad (6)$$

Three fragments A, A' and B have been previously defined for the complexes $[L_2(R)_6 \rightarrow M_3]^{3+}$. In this study, the interaction energies for the fragments A-B and A-BA' in the complexes, $[L_2(R)_6 \rightarrow M_3]^{3+}$; $M = Cu(i), Ag(i), Au(i)$ and $R = C_2H_5, CH_3, H, F,$

Table 5 Natural hybrid orbital (NHO) analysis of $[L_2(R)_6 \rightarrow M_3]^{3+}$ nano-sized complexes

Occupancy	C ₂ H ₅		CH ₃		H		F		Cl		Br		SiH ₃		Ph	
	Au	C	Au	C	Au	C	Au	C	Au	C	Au	C	Au	C	Au	C
Occupancy Au-C	1.96140		1.96240		1.96259		1.95893		1.96252		1.96212		1.95799		1.96057	
%	26.98	73.02	27.17	72.83	27.03	72.97	26.16	73.84	26.42	73.58	26.51	73.49	27.08	72.92	26.54	73.46
% S	75.37	38.64	75.14	38.62	75.02	38.38	75.80	39.41	75.56	39.28	75.43	39.06	75.39	38.53	75.54	39.61
% p	4.37	61.33	4.34	61.35	3.80	61.59	3.90	60.57	4.13	60.69	4.24	60.91	4.32	61.44	4.62	60.36
% d	20.22	0.01	20.48	0.01	21.14	0.01	20.26	0.01	20.28	0.01	20.28	0.01	20.24	0.02	19.79	0.01
% f	0.04	0.01	0.03	0.02	0.04	0.02	0.04	0.02	0.04	0.02	0.04	0.02	0.05	0.02	0.05	0.01



Table 6 Energy decomposition analysis (EDA), (kcal mol⁻¹) of $[L_2(R)_6 \rightarrow M_3]^{3+}$ nano-sized complexes

M	R	Fragment	ΔE_{Pauli}	ΔE_{elstat}	ΔE_{orb}	ΔE_{Dis}	ΔE_{int}
Cu	C ₂ H ₅	A-B	332.9	-462.6(63.6)%	-246.9(33.9)%	-18.4(2.6)%	-395.0
	C ₂ H ₅	A-BA'	319.3	-413.7(67.8)%	-167.6(27.5)%	-28.6(4.7)%	-290.6
	CH ₃	A-B	328.3	-458.7(64.9)%	-239.1(33.9)%	-8.3(1.1)%	-378.1
	CH ₃	A-BA'	315.4	-412.0(68.3)%	-165.8(27.5)%	-25.8(4.2)%	-288.2
	H	A-B	326.6	-454.7(65.1)%	-229.6(32.9)%	-14.4(2.0)%	-372.1
	H	A-BA'	305.9	-408.2(69.3)%	-160.6(27.2)%	-20.6(3.5)%	-283.6
	F	A-B	300.6	-396.2(61.8)%	-231.5(36.1)%	-13.7(2.1)%	-340.7
	F	A-BA'	275.2	-357.5(65.9)%	-165.5(30.5)%	-19.1(3.6)%	-266.9
	Cl	A-B	312.8	-416.8(61.9)%	-241.8(35.9)%	-14.9(2.2)%	-360.8
	Cl	A-BA'	290.3	-375.2(66.3)%	-168.5(29.8)%	-22.4(3.9)%	-275.6
	Br	A-B	314.4	-419.3(61.3)%	-249.2(36.5)%	-15.4(2.2)%	-369.5
	Br	A-BA'	294.0	-377.2(65.9)%	-171.3(29.9)%	-24.00(4.2)%	-278.5
	SiH ₃	A-B	334.3	-459.4(63.1)%	-249.0(34.2)%	-19.7(2.7)%	-393.7
	SiH ₃	A-BA'	322.9	-413.4(67.7)%	-169.7(27.8)%	-27.5(4.5)%	-287.8
Ag	Ph	A-B	330.2	-451.9(61.2)%	-266.0(36.1)%	-20.1(2.7)%	-407.8
	Ph	A-BA'	326.1	-404.6(64.9)%	-177.1(28.4)%	-41.5(6.7)%	-297.2
	C ₂ H ₅	A-B	366.8	-454.30(66.4)%	-212.6(31.0)%	-17.8(2.6)%	-317.9
	C ₂ H ₅	A-BA'	349.2	-419.6(70.2)%	-153.6(25.7)%	-24.4(4.1)%	-248.4
	CH ₃	A-B	363.4	-449.0(66.8)%	-206.8(30.8)%	-16.4(2.4)%	-308.7
	CH ₃	A-BA'	345.4	-416.6(70.6)%	-151.7(25.7)%	-21.8(3.7)%	-244.8
	H	A-B	353.3	-439.4(67.7)%	-195.0(30.1)%	-14.4(2.2)%	-295.6
	H	A-BA'	332.4	-408.1(71.2)%	-146.9(25.6)%	-18.3(3.2)%	-240.9
	F	A-B	328.1	-385.4(64.7)%	-195.3(32.8)%	-115.0(2.5)%	-267.6
	F	A-BA'	304.6	-360.8(68.1)%	-150.4(28.4)%	-18.6(3.5)%	-225.2
	Cl	A-B	344.7	-413.8 (65.1)%	-203.6(32.0)%	-18.40(2.9)%	-291.1
	Cl	A-BA'	320.7	-379.2(68.2)%	-153.5(27.6)%	-23.2(4.2)%	-235.4
	Br	A-B	344.4	-408.9(63.8)%	-212.5(33.1)%	-19.7(3.1)%	-296.8
	Br	A-BA'	324.1	-381.2(67.7)%	-156.4(27.8)%	-25.5(4.5)%	-238.9
Au	SiH ₃	A-B	368.7	-450.2(66.0)%	-212.9(31.2)%	-19.2(2.8)%	-313.5
	SiH ₃	A-BA'	351.8	-418.4(69.7)%	-154.9(25.8)%	-26.7(4.5)%	-248.3
	Ph	A-B	360.2	-442.8(64.1)%	-228.2(33.0)%	-20.1(2.9)%	-330.8
	Ph	A-BA'	655.5	-634.5(71.9)%	-210.1(23.8)%	-37.5(4.3)%	-226.6
	C ₂ H ₅	A-B	553.3	-633.4(62.2)%	-347.9(34.2)%	-36.8(3.6)%	-460.9
	C ₂ H ₅	A-BA'	526.0	-580.3(69.1)%	-228.8(27.3)%	-30.5(3.6)%	-313.6
	CH ₃	A-B	547.8	-626.5(63.5)%	-340.4(34.5)%	-20.0(2.0)%	-439.1
	CH ₃	A-BA'	519.5	-576.9(69.6)%	-226.7(27.3)%	-25.6(3.1)%	-309.8
	H	A-B	546.1	-623.8(64.3)%	-328.5(33.9)%	-17.4(1.8)%	-423.6
	H	A-BA'	509.3	-572.7(70.2)%	-222.3(27.2)%	-21.3(2.6)%	-306.9
	F	A-B	507.7	-551.4(61.5)%	-326.5(36.5)%	-17.9(2.0)%	-388.2
	F	A-BA'	463.5	-506.2(67.0)%	-226.9(30.1)%	-21.6(2.9)%	-291.2
	Cl	A-B	523.4	-575.8(61.5)%	-339.1(36.3)%	-20.1(2.2)%	-412.4
	Cl	A-BA'	488.4	-531.7(67.4)%	-231.1(29.3)%	-26.1(3.3)%	-300.5
R	Br	A-B	549.6	-591.8(61.5)%	-344.7(35.0)%	-24.4(2.5)%	-411.3
	Br	A-BA'	491.2	-533.3(67.1)%	-233.0(29.2)%	-29.4(3.7)%	-304.5
	SiH ₃	A-B	555.1	-630.4(63.0)%	-347.9(34.8)%	-22.6(2.2)%	-445.9
	SiH ₃	A-BA'	531.4	-583.1(69.1)%	-230.9(27.3)%	-30.7(3.6)%	-313.3
	Ph	A-B	545.0	-619.2(61.5)%	-362.6(36.1)%	-24.4(2.4)%	-461.3
	Ph	A-BA'	523.0	-564.6(67.2)%	-234.4(27.9)%	-41.5(4.9)%	-317.5

Cl, Br, Ph and SiH₃, were calculated using the ADF 2013 software at the BP86-D3, TZ2P theoretical level. Optimized output files were used to create the input files for ADF 2013. The results of the energy decomposition analysis (EDA) for the mentioned complexes are presented in Table 6. Assuming that the M₃ remains unchanged, the interaction energy increases as the substituents change from electron-withdrawing to electron-donating. For example, the interaction energy of the $[L_2(F)_6 \rightarrow Au_3]^{3+}$ and $[L_2(Ph)_6 \rightarrow Au_3]^{3+}$ complexes, for the fragments A-B and A-BA' were (-461.36, -387.17) and (-371.51, -291.15) in kcal mol⁻¹, respectively. However, if the substituent

R remains unchanged, the interaction energy exhibits a V-shaped trend, following the order Ag(i) < Cu(i) < Au(i). For instance, the interaction energy of, the $[L_2(C_2H_5)_6 \rightarrow Au_3]^{3+}$, $[L_2(C_2H_5)_6 \rightarrow Ag_3]^{3+}$ and $[L_2(C_2H_5)_6 \rightarrow Cu_3]^{3+}$ complexes for the fragments A-B and A-BA' were (-460.90, -313.57), (-317.88, -248.38) and (-394.96, -290.59) in kcal mol⁻¹, respectively. On the other hand, the highest and lowest interaction energies for A-B fragments in the complexes investigated here correspond to the $[L_2(Ph)_6 \rightarrow Au_3]^{3+}$ and $[L_2(F)_6 \rightarrow Ag_3]^{3+}$ complexes and those for A-BA' fragments are (-461.26, -317.51) and (-267.55, -225.16) in kcal mol⁻¹, respectively. The computational results



align with the interaction energies calculated using Gaussian, at the PBE-D3/def2-TZVP theoretical level. The EDA results indicated that among the three energy decomposition terms in the mentioned complexes, ΔE_{elstat} is the most significant energy term. The values of ΔE_{elstat} for the A–B fragment in the respective complexes of Cu(i), Ag(i) and Au(i) were observed in the ranges of (61.23–65.08) %, (63.78–67.72) %, and (61.53–64.33) %, respectively and for the fragment A–BA' in ranges of (64.92–69.25) %, (67.71–71.93) % and (67.03–70.17) %, respectively. On the other hand the value of ΔE_{orb} in $[\text{L}_2(\text{R})_6 \rightarrow \text{Cu}_3]^{3+}$, $[\text{L}_2(\text{R})_6 \rightarrow \text{Ag}_3]^{3+}$ and $[\text{L}_2(\text{R})_6 \rightarrow \text{Au}_3]^{3+}$ complexes for fragment A–B were (32.87–36.48)%, (30.05–33.14) % and (33.88–36.45) %, respectively, and for the fragment A–BA' were (27.25–30.53)%, (23.81–28.38) % and (27.23–30.06) % respectively. According to the obtained results, the highest and lowest values of the ΔE_{elstat} in the studied complexes for fragment A–B correspond to complexes $[\text{L}_2(\text{H})_6 \rightarrow \text{Ag}_3]^{3+}$, (67.72) % and $[\text{L}_2(\text{Ph})_6 \rightarrow \text{Cu}_3]^{3+}$ (61.23) %, respectively and for fragment A–BA and those correspond to complexes $[\text{L}_2(\text{Ph})_6 \rightarrow \text{Ag}_3]^{3+}$, (71.93) % and $[\text{L}_2(\text{Ph})_6 \rightarrow \text{Cu}_3]^{3+}$, (64.92) %, respectively. The results indicated that the highest and lowest values of ΔE_{orb} for the A–B fragment in the aforesaid complexes correspond to complex $[\text{L}_2(\text{Br})_6 \rightarrow \text{Cu}_3]^{3+}$ with 36.48% (and complex $[\text{L}_2(\text{H})_6 \rightarrow \text{Ag}_3]^{3+}$ with) 30.05%, respectively. For the A–BA' fragment, the highest and lowest values of ΔE_{orb} correspond to complex $[\text{L}_2(\text{F})_6 \rightarrow \text{Cu}_3]^{3+}$ with (30.53) % and complex $[\text{L}_2(\text{Ph})_6 \rightarrow \text{Ag}_3]^{3+}$ with (23.81) %, respectively. The results of the energy decomposition analysis showed that in all studied complexes, the ΔE_{elstat} accounted for the largest share, indicating that the interaction between the fragments is predominantly electrostatic.

EDA-NOCV analysis

NOCV (Natural Orbital for Chemical Valence) provides insights into orbital interactions for asymmetric molecules, as the density of shape changes decomposes the chemical bond into various components (σ , π , δ). The NOCV method indicates the interactions between fragments, which, through energy decomposition calculations, relate to significant orbital interactions between the fragments. Moreover the ΔE_{orb} term can be further analyzed using the NOCV (Natural Orbital for Chemical Valence) extension of the EDA method. The EDA-NOCV approach offers pairwise energy contributions from each set of interacting orbitals to the total bond energy. $\Delta\rho$ refers to the change in electron density between the fragments $\text{L}_2(\text{R})_6$ and M^{3+} . The eigenvalues (ν) give the size of the charge migration. The NOCV analysis for the two fragments, A–B and A–BA', was performed, and the results for the $[\text{L}_2(\text{C}_2\text{H}_5)_6 \rightarrow \text{Au}_3]^{3+}$ complex are presented in Fig. 5. The density of shape between the fragments M^{3+} and $(\text{L}_2(\text{R})_6)$, along with the significant energy results of the remaining complexes $[\text{L}_2(\text{R})_6 \rightarrow \text{M}_3]^{3+}$; $\text{M} = \text{Cu}(\text{i}), \text{Ag}(\text{i}), \text{Au}(\text{i})$ and $\text{R} = \text{C}_2\text{H}_5, \text{CH}_3, \text{H}, \text{F}, \text{Cl}, \text{Br}, \text{Ph}$ and SiH_3 for the fragments A–B and A–BA', is summarized in Fig. S3–S5.† NOCV analysis showed that the types of interactions $\Delta\rho_1$, $\Delta\rho_2$ and $\Delta\rho_3$ present in the $\text{C}_{(\text{tris-NHC})} \rightarrow \text{M}_3$ bond in both fragments A–B and A–BA' were of the σ type, arising from the stable non-bonding electron pairs on the carbon atom. It may be

referred to donation from the non-bonding electron pair of carbon towards the empty d orbital of the metal ions.

Conclusion

In this study, the effect of substituents including: C_2H_5 , CH_3 , H , F , Cl , Br , Ph and SiH_3 on the M–C bond in the nano-sized $[\text{L}_2(\text{R})_6 \rightarrow \text{M}_3]^{3+}$; $[\text{M} = \text{Cu}(\text{i}), \text{Ag}(\text{i}), \text{Au}(\text{i})]$ complexes was investigated at the PBE-D3/def2-TZVP level of theory. The total interaction energies for all mentioned complexes for the fragments AB and A–BA' were also calculated. The interaction energy values for both AB and A–BA' fragments in group 11 metals followed a V-shaped pattern, the trend in energy change observed as $(\text{IE Au}(\text{i}) > \text{IE Cu}(\text{i}) > \text{IE Ag}(\text{i}))$. The cooperativity energy values for the complexes $[\text{L}_2(\text{R})_6 \rightarrow \text{M}_3]^{3+}$; $\text{M} = \text{Cu}(\text{i}), \text{Ag}(\text{i}), \text{Au}(\text{i})$ and $\text{R} = \text{C}_2\text{H}_5, \text{CH}_3, \text{H}, \text{F}, \text{Cl}, \text{Br}, \text{Ph}$ and SiH_3 were calculated. The results indicate that all complexes have positive cooperativity values, suggesting anti-cooperativity. The cooperativity trend for Cu(i), Ag(i), Au(i) metals showed a V-shaped pattern, with the order $\text{Ag}(\text{i}) < \text{Cu}(\text{i}) < \text{Au}(\text{i})$, similar to the trend observed in interaction energies. The natural charge and charge transfer amounts for the complexes $[\text{L}_2(\text{R})_6 \rightarrow \text{M}_3]^{3+}$ with the mentioned substituents were calculated, showing that the charge transfer for the corresponding gold complexes is greater than that for silver, and silver is slightly greater than copper. It seems that in most cases, the complexes with electron-donating substituents have slightly more charge transfer compared to those with electron-withdrawing substituents. Energy decomposition analysis was performed for the two fragments AB and A–BA' in the corresponding complexes. The results showed that in all studied complexes, the ΔE_{elstat} accounted for the largest share, indicating that the interaction between the fragments is predominantly electrostatic. The values of ΔE_{elstat} for fragment A–B in the respective complexes Cu(i), Ag(i) and Au(i) were observed in ranges (61.23–65.08) %, (63.78–67.72) % and (61.53–64.33) % respectively, and for the fragment A–BA' in ranges (64.92–69.25) %, (67.71–71.93) % and (67.03–70.17) %, respectively.

Data availability

The authors confirm that the data supporting the findings of this study are available within the article and its ESI.†

Conflicts of interest

The authors have no conflicts of interest to declare.

References

- 1 S. P. Nolan, *N-heterocyclic Carbenes in Synthesis*, John Wiley & Sons, 2006.
- 2 D. Bourissou, O. Guerret, F. P. Gabbai and G. Bertrand, *Chem. Rev.*, 2000, **100**, 39–92.
- 3 F. Lazreg, F. Nahra and C. S. J. Cazin, *Coord. Chem. Rev.*, 2015, **293–294**, 48–79.



4 F. Wang, L.-j. Liu, W. Wang, S. Li and M. Shi, *Coord. Chem. Rev.*, 2012, **256**, 804–853.

5 T. Zou, C. N. Lok, P. K. Wan, Z. F. Zhang, S. K. Fung and C. M. Che, *Curr. Opin. Chem. Biol.*, 2018, **43**, 30–36.

6 W. Liu and R. Gust, *Chem. Soc. Rev.*, 2013, **42**, 755–773.

7 L. Oehninger, R. Rubbiani and I. Ott, *Dalton Trans.*, 2013, **42**, 3269–3284.

8 W. A. Herrmann, *Angew. Chem. Int. Ed. Engl.*, 2002, **41**, 1290–1309.

9 L. Boselli, M. Carraz, S. Mazères, L. Paloque, G. González, F. Benoit-Vical, A. Valentin, C. Hemmert and H. Gornitzka, *Organometallics*, 2015, **34**, 1046–1055.

10 S. Nayak and S. L. Gaonkar, *ChemMedChem*, 2021, **16**, 1360–1390.

11 M. E. Garner, W. Niu, X. Chen, I. Ghiviriga, K. A. Abboud, W. Tan and A. S. Veige, *Dalton Trans.*, 2015, **44**, 1914–1923.

12 C. Marzano, M. Pellei, F. Tisato and C. Santini, *Anticancer Agents Med. Chem.*, 2009, **9**, 185–211.

13 W. R. Hill and D. M. Pillsbury, *Argyria: the Pharmacology of Silver*, Williams & Wilkins, 1939.

14 S. Medici, M. Peana, G. Crisponi, V. M. Nurchi, J. I. Lachowicz, M. Remelli and M. A. Zoroddu, *Coord. Chem. Rev.*, 2016, **327–328**, 349–359.

15 P. Kumar and I. Cisarova, *J. Organomet. Chem.*, 2013, **735**, 32–37.

16 A. Melaiye, R. S. Simons, A. Milsted, F. Pingitore, C. Wesdemiotis, C. A. Tessier and W. J. Youngs, *J. Med. Chem.*, 2004, **47**, 973–977.

17 F. Hackenberg, G. Lally, H. Müller-Bunz, F. Paradisi, D. Quaglia, W. Streciwick and M. Tacke, *Inorganica Chim. Acta*, 2013, **395**, 135–144.

18 S. Patil, K. Dietrich, A. Deally, B. Gleeson, H. Müller-Bunz, F. Paradisi and M. Tacke, *Helv. Chim. Acta*, 2010, **93**, 2347–2364.

19 V. Gandin, M. Pellei, M. Marinelli, C. Marzano, A. Dolmella, M. Giorgetti and C. Santini, *J. Inorg. Biochem.*, 2013, **129**, 135–144.

20 G. J. Higby, *Gold Bull.*, 1982, **15**, 130–140.

21 I. C. Shaw, *Chem. Rev.*, 1999, **99**, 2589–2600.

22 P. J. Barnard, M. V. Baker, S. J. Berners-Price and D. A. Day, *J. Inorg. Biochem.*, 2004, **98**, 1642–1647.

23 O. Sanchez, S. González, M. Fernández, A. R. Higuera-Padilla, Y. Leon, D. Coll, A. Vidal, P. Taylor, I. Urdanibia, M. C. Goite and W. Castro, *Inorganica Chim. Acta*, 2015, **437**, 143–151.

24 R. W. Sun, M. Zhang, D. Li, Z. F. Zhang, H. Cai, M. Li, Y. J. Xian, S. W. Ng and A. S. Wong, *Chemistry*, 2015, **21**, 18534–18538.

25 J. Weaver, S. Gaillard, C. Toye, S. Macpherson, S. P. Nolan and A. Riches, *Chemistry*, 2011, **17**, 6620–6624.

26 P. de Frémont, E. D. Stevens, M. D. Eelman, D. E. Fogg and S. P. Nolan, *Organometallics*, 2006, **25**, 5824–5828.

27 C. H. G. Jakob, A. W. Muñoz, J. F. Schlagintweit, V. Weiß, R. M. Reich, S. A. Sieber, J. D. G. Correia and F. E. Kühn, *J. Organomet. Chem.*, 2021, 932.

28 J. Rieb, B. Dominelli, D. Mayer, C. Jandl, J. Drechsel, W. Heydenreuter, S. A. Sieber and F. E. Kuhn, *Dalton Trans.*, 2017, **46**, 2722–2735.

29 M. Rezaeivala, M. Ahmadi, B. Captain, M. Bayat, M. Saeidirad, S. Şahin-Bölükbaşı, B. Yıldız and R. W. Gable, *Inorganica Chim. Acta*, 2020, **513**, 119935.

30 B. Naderizadeh and M. Bayat, *ACS Omega*, 2020, **5**, 26999–27015.

31 B. Naderizadeh and M. Bayat, *Mendeleev Commun.*, 2021, **31**, 179–181.

32 B. Naderizadeh, M. Bayat, M. Ranjbaran and S. Salehzadeh, *J. Mol. Liq.*, 2021, **341**, 117310.

33 B. Naderizadeh and M. Bayat, *J. Iran. Chem. Soc.*, 2024, 1–24.

34 A. Rit, T. Pape and F. E. Hahn, *J. Am. Chem. Soc.*, 2010, **132**, 4572–4573.

35 A. Rit, T. Pape, A. Hepp and F. E. Hahn, *Organometallics*, 2010, **30**, 334–347.

36 J. P. Perdew, M. Ernzerhof and K. Burke, *J. Chem. Phys.*, 1996, **105**, 9982–9985.

37 S. Grimme, J. Antony, S. Ehrlich and H. Krieg, *J. Chem. Phys.*, 2010, **132**, 154104.

38 F. Weigend and R. Ahlrichs, *Phys. Chem. Chem. Phys.*, 2005, **7**, 3297–3305.

39 M. J. Frisch, G. W. Trucks, H. B. Schlegel, G. E. Scuseria, M. A. Robb, J. R. Cheeseman, G. Scalmani, V. Barone, B. Mennucci, G. A. Petersson, H. Nakatsuji, M. Caricato, X. Li, H. P. Hratchian, A. F. Izmaylov, J. Bloino, G. Zheng, J. L. Sonnenberg, M. Hada, M. Ehara, K. Toyota, R. Fukuda, J. Hasegawa, M. Ishida, T. Nakajima, Y. Honda, O. Kitao, H. Nakai, T. Vreven, J. A. Montgomery Jr, J. E. Peralta, F. Ogliaro, M. Bearpark, J. J. Heyd, E. Brothers, K. N. Kudin, V. N. Staroverov, R. Kobayashi, J. Normand, K. Raghavachari, A. Rendell, J. C. Burant, S. S. Iyengar, J. Tomasi, M. Cossi, N. Rega, J. M. Millam, M. Klene, J. E. Knox, J. B. Cross, V. Bakken, C. Adamo, J. Jaramillo, R. Gomperts, R. E. Stratmann, O. Yazayev, A. J. Austin, R. Cammi, C. Pomelli, J. W. Ochterski, R. L. Martin, K. Morokuma, V. G. Zakrzewski, G. A. Voth, P. Salvador, J. J. Dannenberg, S. Dapprich, A. D. Daniels, Ö. Farkas, J. B. Foresman, J. V. Ortiz, J. Cioslowski and D. J. Fox, *Gaussian 09, Revision D.01*, Gaussian, Inc., Wallingford CT, 2009.

40 M. Bayat, F. Amraie and S. Salehzadeh, *J. Theor. Comput. Chem.*, 2016, **15**(4), 1650032.

41 S. Salehzadeh and F. Maleki, *J. Comput. Chem.*, 2016, **37**, 2799–2807.

42 H. S. Frank and W.-Y. Wen, *Faraday Discuss. R. Soc. Chem.*, 1957, **24**, 133–140.

43 I. Alkorta, F. Blanco, P. M. Deyà, J. Elguero, C. Estarellas, A. Frontera and D. Quiñonero, *Theor. Chem. Acc.*, 2009, **126**, 1–14.

44 D. Hankins, J. W. Moskowitz and F. H. Stillinger, *Chem. Phys. Lett.*, 1970, **4**, 527–530.

45 Q. Li, H. Liu, X. An, B. Gong and J. Cheng, *J. Mol. Struct. THEOCHEM*, 2008, **861**, 14–17.



46 C. Estarellas, A. Frontera, D. Quinonero, I. Alkorta, P. M. Deya and J. Elguero, *J. Phys. Chem. A*, 2009, **113**, 3266–3273.

47 D. Escudero, C. Estarellas, A. Frontera, D. Quiñonero and P. M. Deyà, *Chem. Phys. Lett.*, 2010, **485**, 221–225.

48 C. Estarellas, A. Frontera, D. Quinonero and P. M. Deya, *ChemPhysChem*, 2011, **12**, 2742–2750.

49 M. Solimannejad, *ChemPhysChem*, 2012, **13**, 3158–3162.

50 M. Solimannejad, Z. Rezaei and M. D. Esrafil, *J. Mol. Model.*, 2013, **19**, 5031–5035.

51 M. D. Esrafil, P. Esmailpour, F. Mohammadian-Sabet and M. Solimannejad, *Chem. Phys. Lett.*, 2013, **588**, 47–50.

52 B. Gong, B. Jing, Q. Li, Z. Liu, W. Li, J. Cheng, Q. Zheng and J. Sun, *Theor. Chem. Acc.*, 2009, **127**, 303–309.

53 X. Guo, Y.-W. Liu, Q.-Z. Li, W.-Z. Li and J.-B. Cheng, *Chem. Phys. Lett.*, 2015, **620**, 7–12.

54 Q. Li, R. Li, Z. Zhou, W. Li and J. Cheng, *J. Chem. Phys.*, 2012, **136**, 014302.

55 W. Wang and Q. Li, *Comput. Theor. Chem.*, 2011, **977**, 128–133.

56 A. Whitty, *Nat. Chem. Biol.*, 2008, **4**, 435–439.

57 M. F. Perutz, *Q. Rev. Biophys.*, 1989, **22**, 139–237.

58 S. S. Movafagh and S. Salehzadeh, *Phys. Chem. Chem. Phys.*, 2024, **26**, 15005–15017.